STABILITIY ANALYSIS OF CONSTANT-FREQUENCY CURRENT-MODE CONTROLLED SWITCHING REGULATORS OPERATING ABOVE 50% DUTY RATIO

Richard Redl

Istvan Novak

Technical University of Budapest
POB 91, Budapest, Hungary H-1502

ABSTRACT

Extension of the analysis of the constant-frequency current-mode controlled switching voltage regulators to operation above 50% duty ratio is presented. As it is known, stable behavior above 50% can be achieved at open voltage regulating loop by employing an external ramp for compensation but the possibility of instabilities at closed voltage regulating loop still exists. Calculation of the maximum usable ac loop gain is accomplisned by taking into account the amplified and fed-back output ripple voltage. Both the continuous and hysteretic instabilities are discussed and diagrams to facilitate the design of the optimum error processor are given. Experiments carried out on the buck and boost converters support the derived results.

1. INTRODUCTION

The popularity of the current-mode control of switching voltage regulators has been steadily increasing. This method, which bears a number of different names (e. g. "Current-Programmed Mode", "Peak-Current Control", "Current-Injected Control" "Current-Controlled Modulation", etc.), yields several very advantageous characteristics as compared to other two-loop controlling methods or to the traditional pulse-width modulation. These characteristics (single-pole control transfer function, smooth pulse-by-pulse overcurrent limiting, easy paralleling of power stages with automatic current sharing, possibility of feed-forward of input voltage and/or output current for nearly ideal transient response [10]) are equally desirable in almost all types of power supplies: in laboratory instruments, in OEM modular power supplies and at very high power and high reliablility applications, including spacecraft and military electronics. Current-mode control emerges in off-line switching power supplies with unity power factor and in sine - wave power inverters, too.

Depending on the type of the employed pulse modulator several different versions of current-mode control can be distinguished. (For a compilation of the most frequent circuit solutions see e.g. [1].) Indisputably, the constant-frequency peak-current controller has the largest practical importance among the possible variations. EMC considerations, elimination of the acoustic noise, application of transformer in the power stage, synchronization requirements, etc, call for constant-frequency operation.

So our attention will be focused on this particular controller type. Previous studies [2]-[6] dealt with the low-frequency stability problems of the constant-frequency current-mode controlled converters and some [7],[1] discussed the effect of fed-back ripple voltage on the high frequency operation (the term "high frequency" is used here for the clock frequency component and its lower-order subharmonics). It was shown that the fed-back ripple can cause hysteretically or continuously arising subharmonic instability and this imposes an upper limit on the applicable loop gain. There is, however, a missing topic in the discussion: the effect of ripple feedback on the operation above 50% duty ratio. It is long known [8] that at duty ratios above 50% the constant-frequency peak-current controller displays instability even with open voltage regulating loop. Deisch proposed a method to overcome this problem [9]. The solution is to add a stabilizing ramp to the sensed current thus providing the proper current slope ratios. But until now the effect of ripple feedback on this slope compensated case has not been analysed. Our intention with this paper is to complete the description of the current mode control by extending the high frequency stability analysis above 50%.

The block schematic of a power converter with slope compensated current-mode controller is shown in Fig.1. The operation is as follows. The switch (or switches in push-pull and other multi-switch topologies) is turned off by resetting the R-S latch with the output of the current comparator. This happens if the sum of the sensed switch or

inductor current and the compensating ramp i_c exceeds the error signal i_e. Conduction of the switch starts again when the next clock pulse sets the latch. Regulation of the output voltage against load or line variations is provided by varying the control signal, which in our case is the same as the output of the error amplifier (i_e).

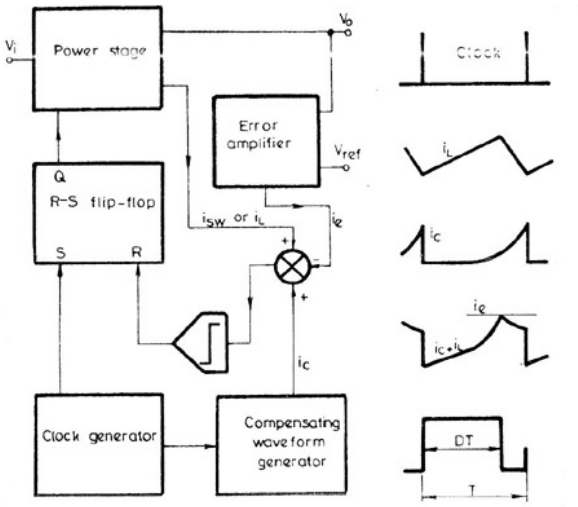

Fig.1. Slope-compensated constant-frequency current-mode controller

The following questions have to be answered at the circuit of Fig.1. First: what is the optimum wave-shape for the compensating ramp? Second: what is the maximum usable transfer conductance of the error amplifier? (Usable conductance means here that the voltage feedback loop does not produce instability.)

1.1. Determination of the compensating ramp

It can be easily shown [3] that in the converter, whose block schematic is shown in Fig.1, any perturbation in the current minimum of the inductor propagates from cycle to cycle as

$$\Delta I_n = -\frac{m_2 - m_c}{m_1 + m_c}\,\Delta I_{n-1} \qquad /1/$$

where

m_1: slope of the rising inductor current;
m_2: slope of the falling inductor current (absolute value);
m_c: slope of the compensating ramp at the moment of turn-off.

Perturbations don't increase if the absolute value of the multiplier of ΔI_{n-1} is not more than 1. Expressing m_c/m_2 and solving the resultant differential equation results in the Deisch function [9]:

$$f_c(t) = \begin{cases} \frac{T}{2}\left(2\frac{t}{T} - \ln\frac{t}{T} - \ln 2e\right) & \text{for } t > \frac{T}{2} \\ 0 & \text{for } t \le \frac{T}{2} \end{cases} \qquad /2/$$

Here T is the clock period time and e is the base of the natural logarithm.

For a regulated buck converter m_2 can be considered to be constant. Therefore the required compensating ramp can be written as

Buck:

$$i_c = \begin{cases} \frac{V_o T}{2L}\left(2\frac{t}{T} - \ln\frac{t}{T} - \ln 2e\right) & \text{for } t > \frac{T}{2} \\ 0 & \text{for } t \le \frac{T}{2} \end{cases} \qquad /3/$$

where V_o: output voltage (diode forward voltage drop neglected);
L : inductance of filter inductor.

Similar considerations result for the boost and the buck-boost converters in:

Boost:

$$i_c = \begin{cases} \frac{V_o T}{2L}\left[\left(\frac{t}{T}\right)^2 - \frac{t}{T} + \frac{1}{4}\right] & \text{for } t > \frac{T}{2} \\ 0 & \text{for } t \le \frac{T}{2} \end{cases} \qquad /4/$$

Buck-boost:

$$i_c = \begin{cases} -\frac{V_o T}{2L}\left(2\frac{t}{T} - \ln\frac{t}{T} - \ln 2e\right) & \text{for } t > \frac{T}{2} \\ 0 & \text{for } t \le \frac{T}{2} \end{cases} \qquad /5/$$

The waveforms of these compensating ramps are shown in Fig.2.

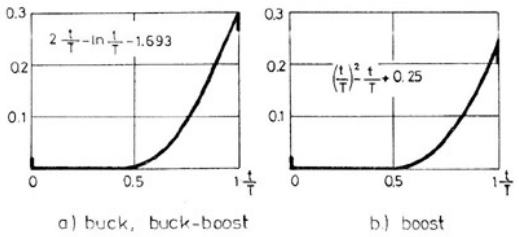

Fig.2. Compensating ramps to ensure marginal open-loop stability

However the application of these ramps produces only marginal open-loop stability, that is the perturbations neither increase in amplitude nor settle down. It is a better choice to employ a compensating ramp which eliminates any perturbation in the inductor current as fast as possible. The obvious choice for the ramp slope is [3], [6]

$$m_{c\ opt} = m_2 \qquad /6/$$

which gives zero multiplying factor for the perturbation. By a ramp having the slope as in Eq. /6/ any perturbation disappears within one cycle. The optimum ramp can be also easily calculated. For the three basic topologies its time function is given subsequently (here also, it is assumed that the output voltage is constant, and the duty ratio varies according to the input voltage variations).

Buck:
$$i_{c\ opt} = \frac{V_o T}{2L}\left(\frac{2t}{T}\right) \qquad 0<t<T \qquad /7/$$

Boost:
$$i_{c\ opt} = \frac{V_o T}{2L}\left[2\left(\frac{t}{T}\right)^2\right] \qquad 0<t<T \qquad /8/$$

Buck-boost:
$$i_{c\ opt} = \frac{V_o T}{2L}\left(\frac{2t}{T}\right) \qquad 0<t<T \qquad /9/$$

These waveforms are shown in Fig.3.

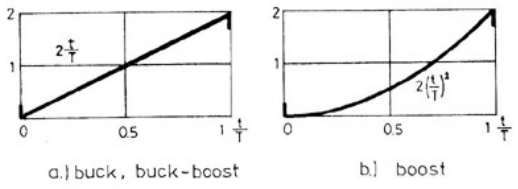

a.) buck, buck-boost b.) boost

Fig.3. Compensating ramps to ensure optimum open-loop stability

It is worth to note that the use of ramps which are larger than those, producing marginal stability, has a significant effect on the static current limiting characteristic of the converter. The effect is an increase in the short circuit-current as compared to the nominal maximum output current. This increase results in extra current stress on the power handling components, too. For illustration: the increase in the short-circuit current and in the switch peak current can be as high as half of the maximum operational ripple current in the filter inductor for a buck converter with optimum compensation. However, this effect, if undesirable, can be eliminated by using some type of foldback current limiting.

1.2. Maximum usable gain

The knowledge of the maximum usable gain is important for two reasons. First: instable operation, i.e. oscillation in the voltage regulating loop is inadmissible and must be avoided in most practical cases. Second: dc regulation and dynamic performance often require high loop gain. Although in a number of applications integral feedback can be used with practically infinite dc loop gain, thus providing superior static performance, proper dynamic response can be achieved only above certain ac gain value of the voltage regulating loop. There are also cases when use of the integral feedback is not desirable. If the load is, for instance, a constant current sink an integral feedback produces zero phase margin below the corner frequency of the error amplifier. Varying load also makes impossible to match its pole to the zero of the error amplifier. This is illustrated by Fig.4., where the model of a current-mode controlled converter and the characteristic Bode plots can be seen.

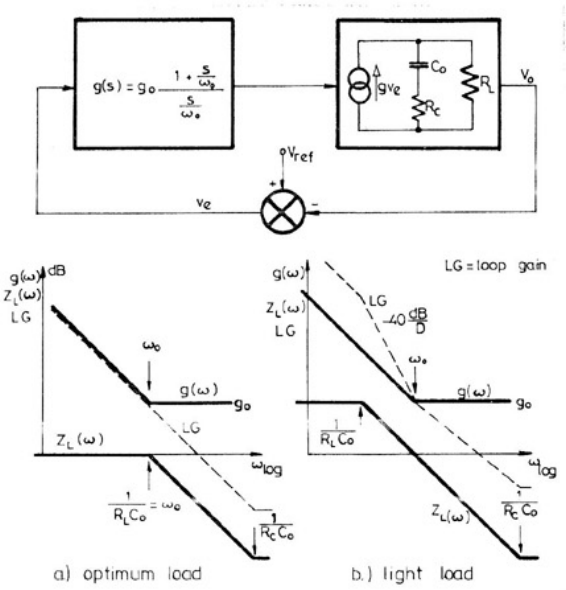

a) optimum load b.) light load

Fig.4. Model of voltage feedback loop and the relevant Bode plots

Optimum load (a) can produce an open loop response which is similar to that of the ideal integrator with an associated 90° phase margin. Light load (b), however, can produce -40 dB/decade slope of the loop gain between the pole of the load impedance and the zero of the error amplifier with virtually zero degree phase margin. If there are other phase shifting elements in the system or smooth transient response is a requirement the integrating frequency re-

sponse of the error amplifier has to be changed, and constant transconductance must be provided. This, however, deteriorates the static regulation which calls again for the use of the maximum possible gain.

Our goal is to determine the value of this gain in order to facilitate the design of the control loop. The until now not analysed case (constant-frequency peak-current controller above 50% duty ratio) is the subject of our investigations. The method used throughout the analysis, was introduced in [1], so only the main points will be repeated here.

2. CONTINUOUS SUBHARMONIC INSTABILITY

Increasing the gain of the error amplifier can result in subharmonic instability at the constant-frequency peak-current controlled converters. If the gain values, where subharmonic oscillation starts and stops, are equal we have the case of continuous instability.

The gain at the boundary of instability can be calculated by the perturbation method described in [1]. The brief summary of the method is the following. Let $\underline{u}$ be the vector of infinitesimal perturbations injected in the state variables of the system. The response vector $\underline{v}$ is given by the matrix equation

$$\underline{v} = \underline{\underline{A}}\,\underline{u} \qquad /10/$$

The matrix $\underline{\underline{A}}$ is determined by the circuit parameters of the system, including duty ratio and error amplifier transconductance. The system is locally stable, that is small perturbations settle down, if the absolute value of the eigenvalue λ of matrix $\underline{\underline{A}}$ is smaller than 1. λ can be calculated from the characteristic equation

$$[\underline{\underline{A}} - \lambda\underline{\underline{I}}] = 0 \qquad /11/$$

where $\underline{I}$ is the identity matrix.

Assuming first order subharmonic oscillation of infinitesimal amplitude (λ=-1), the characteristic equation can be written in the from:

$$1+a_{11}+a_{22}+a_{11}a_{22}-a_{12}a_{21}=0 \qquad /12/$$

Eq./12/ is suitable for the calculation the critical transconductance of the error amplifier.

2.1. Determination of the matrix elements

The determination of the matrix elements will be shown for the buck regulator. Two state variables will be assumed: the current in the filter inductor and the voltage in the filter capacitor. The circuit model with the generators, which represent the perturbations of the state variables, is shown in Fig.5.

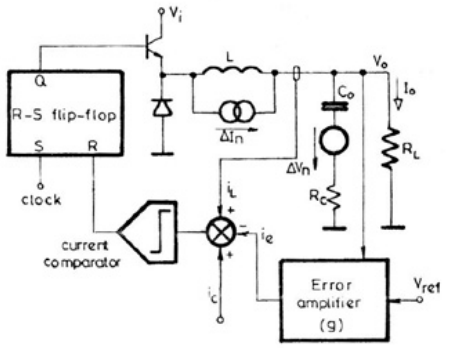

Fig.5. Buck regulator with perturbations

For the analysis $\underline{u}$ and $\underline{v}$ are given as

$$\underline{u} = \begin{bmatrix} \Delta I_n \\ \Delta V_n \end{bmatrix} ; \qquad \underline{v} = \begin{bmatrix} \Delta I_{n+1} \\ \Delta V_{n+1} \end{bmatrix} \qquad /13/$$

We assume that the perturbations enter at the beginning of the nth period and the response vector is measured at the beginning of the (n+1)th period. The matrix elements are to be calculated with special excitations, according to their definitions

$$a_{11}=\left.\frac{\Delta I_{n+1}}{\Delta I_n}\right|_{\Delta V_n=0} \qquad a_{12}=\left.\frac{\Delta I_{n+1}}{\Delta V_n}\right|_{\Delta I_n=0}$$

$$a_{21}=\left.\frac{\Delta V_{n+1}}{\Delta I_n}\right|_{\Delta V_n=0} \qquad a_{22}=\left.\frac{\Delta V_{n+1}}{\Delta V_n}\right|_{\Delta I_n=0} \qquad /14$$

For the calculations a closer look at the waveforms of the current comparator is necessary (Fig.6). Turn-off happens when the sum of the inductor current i_L and the compensating current i_c equals the current from the error amplifier i_e. Details around the turn-off instant with and without perturbation in the inductor current are enlarged in Fig.7.

From geometrical considerations we get

$$\Delta T_n = \frac{\Delta I_n + \Delta I_e}{m_1 + m_c - m_e} \qquad /15/$$

where

$$\Delta I_e = g\Delta I_n\left(R_c + \frac{DT}{C_o}\right) \qquad /16/$$

and m_e is the slope of i_e at turn-off.

The perturbation in the inductor current at the end of the nth period is given as

$$\Delta I_{n+1} = \Delta I_n - m_1 \Delta T_n + m_2 \Delta T_n \qquad /17/$$

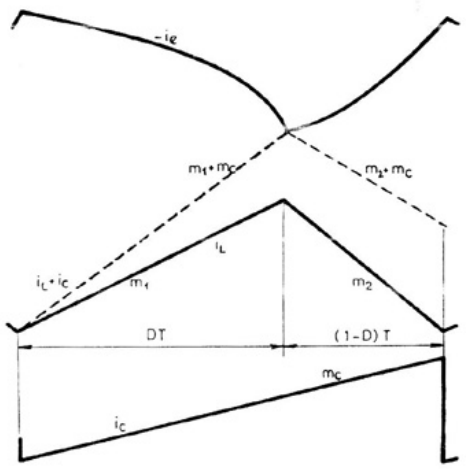

Fig.6. Waveforms of the current comparator in steady state

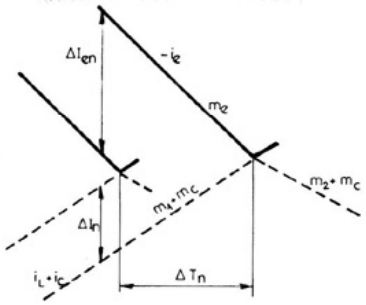

Fig.7. Waveforms in the vicinity of the turn-off instant at current perturbation

The perturbation in the capacitor voltage can be also calculated

$$\Delta V_{n+1} = \frac{\Delta I_n DT}{C_o} + \frac{\Delta I_{n+1}(1-D)T}{C_o} \qquad /18/$$

Combining Eqs. /15/, /16/ and Eqs. /17/, /18/ and using the definitions under /14/ we arrive at

$$a_{11} = 1 - \frac{m_1 - m_2}{m_1 + m_c - m_e}\left[1 + g\left(R_c + \frac{DT}{C_o}\right)\right] \qquad /19/$$

and

$$a_{21} = \frac{DT}{C_o} + \frac{(1-D)T}{C_o} a_{11} \qquad /20/$$

The remaining matrix elements are determined from Fig.8.

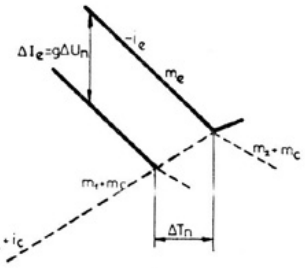

Fig.8. Waveforms in the vicinity of the turn-off instant at voltage perturbation

Here

$$\Delta T_n = \frac{\Delta I_e}{m_1 + m_c - m_e} = \frac{g\Delta V_n}{m_1 + m_c - m_e} \qquad /21/$$

and

$$\Delta I_{n+1} = (m_2 - m_1)\Delta T_n \qquad /22/$$

So

$$a_{12} = g\,\frac{m_2 - m_1}{m_1 + m_c - m_e} \qquad /23/$$

At last a_{22} comes from the equation

$$\Delta V_{n+1} = \frac{\Delta I_{n+1}(1-D)T}{C_o} + \Delta V_n \qquad /24/$$

from where

$$a_{22} = 1 + g\,\frac{(m_2 - m_1)(1-D)T}{(m_1 + m_c - m_e)C_o} \qquad /25/$$

Similar consideration apply for the boost converter and other cicuit versions, too. The matrix elements for the buck, boost and buck-boost converters are collected in Table 1. Table 2 shows the expressions for the slopes of the inductor current and the amplified feedback ripple (m_e). Here D' = 1 - D.

2.2. Characteristic equation

Substituting the expressions for the matrix elements and slopes from Tables 1 and 2 in Eq. /12/ we get the characteristic equation for the system. This equation can be solved for the maximum usable transconductance g of the error amplifier or for the compensating slope m_c. The compensating slope, however, is usually selected according to the considerations of Section 1.1.

The characteristic equation is a quadratic equation for g:

$$Ag^2 + Bg + C = 0 \qquad /26/$$

TABLE 1. PERTURBATION MATRICES (A_n) FOR THE SLOPE-COMPENSATED CASE

$$\text{Buck}\quad \begin{bmatrix} 1-\frac{m_1 m_2}{m_1+m_c-m_e}\left[1+g\left(R_c+\frac{DT}{C_o}\right)\right] & g\frac{m_2-m_1}{m_1+m_c-m_e} \\ \frac{DT}{C_o}+\frac{D'T}{C_o}a_{11} & 1+\frac{D'T}{C_o}a_{12} \end{bmatrix}$$

$$\text{Boost}\quad \begin{bmatrix} \frac{m_2+m_c-m_e}{m_1+m_c-m_e} & g\frac{m_2-m_1}{m_1+m_c-m_e} \\ \frac{D'T}{C_o}a_{11} & 1+\frac{D'T}{C_o}a_{12} \end{bmatrix}$$

$$\text{Buck-boost}\quad \begin{bmatrix} \frac{m_2-m_c-m_e}{m_1+m_c-m_e} & g\frac{m_2-m_1}{m_1+m_c-m_e} \\ \frac{D'T}{C_o}a_{11} & 1+\frac{D'T}{C_o}a_{12} \end{bmatrix}$$

TABLE 2. SLOPES OF INDUCTOR CURRENT AND FEEDBACK RIPPLE

	m_1	m_2	m_e
Buck	$\frac{V_o D'}{LD}$	$-\frac{V_o}{L}$	$-g\frac{V_o D'}{LD}(R_c+\frac{DT}{2C_o})$
Boost	$\frac{V_o D'}{L}$	$-\frac{V_o D}{L}$	$g\frac{I_o}{C_o}$
Buck-Boost	$-\frac{V_o D'}{LD}$	$\frac{V_o}{L}$	$-g\frac{I_o}{C_o}$

Significant simplification in the coefficients of Eq. /26/ can be achieved by introducing new, dimensionless variables. The new variables are:

for the buck converter:

$$g' = gR_c \quad \text{and} \quad r = \frac{T}{R_c C_o} \qquad /27/,\ /28/$$

for the boost and buck-boost converter:

$$g' = g\frac{L}{R_L C_o} \quad \text{and} \quad r = \frac{TR_L}{L} \qquad /29/,\ /30/$$

(R_L: load resistance)

for all three converters:

$$m' = m_c \frac{V_o}{L} \qquad /31/$$

The new quadratic equation will have the from

$$A'g'^2 + B'g' + C' = 0 \qquad /32/$$

The coefficients of this equation are collected in Table 3.

TABLE 3. COEFFICIENTS OF EQ. (32)*

	A'	B'	C'
Buck	$2-6D+4D^2+$ $+r(-1+4D-7D^2+4D^3)+$ $+r^2(-\frac{D}{2}+\frac{3D^2}{2}-2D^3+D^4)$	$4-12D+8D^2+$ $+m'(6D-8D^2)+$ $+r[-1+4D-7D^2+4D^3+$ $+m'(-D+4D^2-4D^3)]$	$2-6D+4D^2+$ $+m'(6D-8D^2)+$ $+4m'^2D^2$
Boost	$4+rD'$	$-6+8D-rD'^2-m'(6+rD')$	$2-6D+4D^2$ $+m'(6-8D)+$ $+4m'^2$
Buck-Boost	$4D^2+rDD'$	$-6D+8D^2-rD'^2+$ $+m'(D+7D^2)$	$2-6D+4D^2+$ $+m'(-6D+8D^2)+$ $+4m'^2D^2$

* For definitions of r and m' see the text

As it can be seen, Eq. /32/ is quadratic not only for the transconductance but for the compensating slope, too. So at a given duty ratio either of them can be easily calculated. In contrary to the uncompensated case coefficient C' does not disappear at 50% duty ratio, that is finite g' is allowed, just as it was expected from direct analysis of the propagation conditions of perturbations at open voltage regulating loop.

3. HYSTERETIC SUBHARMONIC INSTABILITY

As it has been mentioned elsewhere [7], [1], constant-frequency current-mode controlled converters are subjected to hysteretic subharmonic oscillation, too. The appearance of this particular instability is a hysteretic function of the transconductance of the error amplifier, that is the system jumps into subharmonic oscillation at a higher gain and abandons oscillation at a lower gain. The amplitude of the oscillation, if present, does not depend on the loop gain.

The physical reason of the hysteretic instability is the following. If the loop gain is high enough to produce a fed-back ripple, which does not allow the change of the current comparator at the arrival of the next clock pulse, the system omits one

conduction period, and subharmonic oscillation starts. Because of the subharmonic oscillation the output and also the fed-back ripple increase in amplitude and this prevents the system from returning to normal operation.

Hysteretic instability is predictable and calculations and experiments carried out for the uncompensated case show good agreement (see e.g. Fig.17 in [1]).

It is also rather easy to determine the upper gain limit for the compensated case. However there are some difficulties with the prediction of the lower limit. The reason is simple: if the system enters subharmonic oscillation the nature of compensation changes (ramp starts somewhere in the middle of the new period) and though calculation can be done, a number of different subcases must be considered. A complete discussion of all possible situations is beyond the scope of this paper, so only the determination of the upper limits will be shown. Also the discussion of the buck converter will be omitted, because here hysteretic instability is impossible - the fed-back ripple is always above the inductor current at the end of the period.

At the boost and buck-boost converters there are two subcases, according to the turn-on condition. If there is an unconditional turn-on at the arrival of the clock pulse we speak about dynamic turn-on. If, however, turn-on can occur only if the fed-back ripple is below the sum of the inductor current and compensating current, static turn-on condition exists.

The main difference is that at dynamic turn-on a small voltage jump on the ESR of the filter capacitor appears during the presence of the clock pulse and this alters the gain limit where the system enters hysteretic subharmonic oscillation.

For illustration the derivation of the upper gain limit at static turn-on will be presented for the boost converter. The characteristic waveshapes at the input of the current comparator are shown in Fig.9.

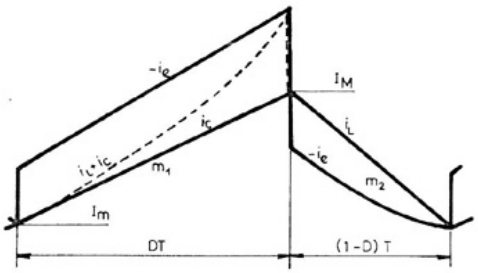

Fig.9. Current comparator waveforms of a boost converter with slope compensation at the verge of hysteretic oscillation (static turn-on)

It is assumed that the compensating ramp is inhibited at the turn-off instant.

The condition of instability is that the amplified and fed-back ripple ($-i_e$) be equal to the inductor current at the end (or what is the same) at the beginning of the period. That is

$$g\left(\frac{I_o DT}{C_o} + I_m R_c\right) = m_1 DT + i_c(DT) \qquad /33/$$

Here the following relations hold:

$$I_m = \frac{I_o}{D'} - \frac{TV_o}{2L} DD' \qquad /34/$$

and

$$m_1 = \frac{V_o D'}{L} \qquad /35/$$

Substituting /34/ and /35/ into /33/ and expressing g results in

$$g = \frac{DD' \frac{V_o T}{L} + i_c(DT)}{\frac{DTI_o}{C_o} + R_c\left(\frac{I_o}{D'} - \frac{V_o T}{2L} DD'\right)} \qquad /36/$$

Similar considerations apply for the buck-boost converter and for the case of dynamic turn-on, too. The results are collected in Table 4.

TABLE 4. TRANSCONDUCTANCES AT THE START OF HYSTERETIC SUBHARMONIC OSCILLATION

	STATIC TURN-ON	DYNAMIC TURN-ON
Boost	$g = \frac{DD' \frac{V_o T}{L} + i_c(DT)}{\frac{DTI_o}{C_o} + R_c\left(\frac{I_o}{D'} - \frac{V_o T}{2L} DD'\right)}$	$g = \frac{DD' \frac{V_o T}{L} + i_c(DT)}{\frac{DTI_o}{C_o}}$
Buck-boost	$g = \frac{-D' \frac{V_o T}{L} + i_c(DT)}{\frac{DTI_o}{C_o} + R_c\left(-\frac{I_o}{D'} + \frac{V_o T}{2L} D'\right)}$	$g = \frac{-D' \frac{V_o T}{L} + i_c(DT)}{\frac{DTI_o}{C_o}}$

4. DESIGN PROCEDURE

The results summarized in Sections 2 and 3 make possible the direct design of a current-mode controlled converter which is free from subharmonic instability. The usual procedure is indicated in Fig. 10.

The computation begins with the determination of the minimum and maximum duty ratios and with calculation of the inductance (and transformer parameters in the transformer-copupled versions). Capacitance of the filter capacitor and its equivalent series resistance can be calculated from the maximum allowable output ripple voltage. Dynamic and static regulation de-

termine the overall loop gain and the zero of the error amplifier.

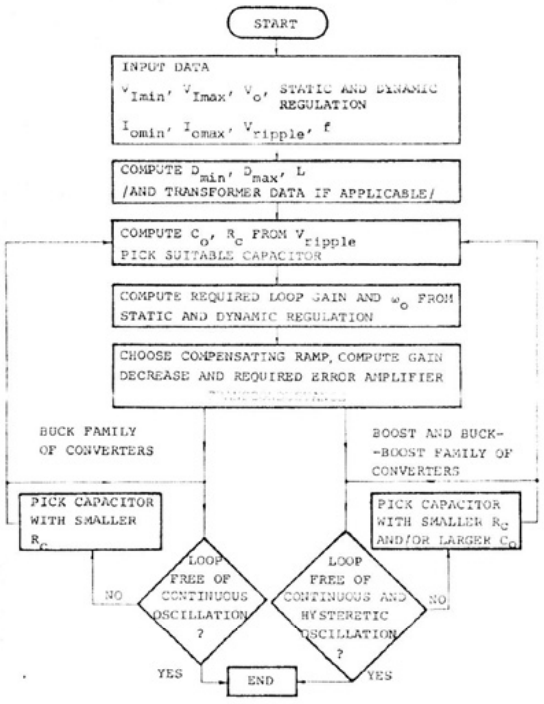

Fig.10. Algorithm for the design of a contant-frequency peak-current controlled converter

Next step is the selection of the compensating ramp and calculation of the required transconductance of the error amplifier. (The application of the compensating ramp decreases the overall loop gain, this will be determined later.) Eventually checking of the loop stability follows. At the buck and buck derived family of converters this must be done for only the continuous type of oscillation, however at the boost, buck-boost and other flyback converters it must be accomplished for both the continuous and hysteretic oscillation. If oscillation can occur and there is no way to decrease the loop gain new capacitor with smaller ESR and/or larger capacitance must be selected.

As it was mentioned before the compensating ramp decreases the loop gain. It is easy to show that the amount of gain decrease is given by

$$a = \frac{m_1}{m_1 + m_c} \qquad /37/$$

so the required transconductance of the error amplifier must be larger then that, resulting in from the regulation requirements, by the reciprocal of a.

From the viewpoint of continuous instability the power stage of a converter can be characterized by only one parameter $r=T/R_cC_o$ which was introduced in Section 2.2. In order to facilitate the control loop design some sample calculations were done and the results are submitted in the form of diagrams. Fig.11. shows the normalized transconductances ($g' = gR_c$) of the buck regulator at the verge of oscillation for different r and different $m' = m_cV_o/L$ values with D as independent variable.

Fig.12. collects results of similar calculations for the boost regulator. Here $g' = gLI_o/C_oV_o$ and $r = TV_o/LI_o$.

Fig.13. is a special design aid for the buck and boost converters. It displays g' at the optimum compensation ramps of Fig.3. The optimum ramp is linear with $m' = 1$ for the buck converter and it is parabolic with $m' = D$ for the boost converter.

5. EXPERIMENTAL RESULTS

A constant-frequency peak current controlled circuit having slope compensation capability was built and measurements were carried out for two different power stages (a buck and a boost converter). The parameters of the experimental circuits are collected in Table 5.

TABLE 5. PARAMETERS OF EXPERIMENTAL CIRCUITS

	Buck			Boost	
V_o [V]	10			20	
I_o [mA]	910			360	
L [μH]	507			507	
T [μsec]	58	54,5	54,5	50	50
C_o [μF]	134	44,5	44,5	532	532
R_c [mΩ]	210	245	245	42	280
m_c [A/μsec]	19,7	19,7	9,9	46,2	46,2
$D_1^{(1)}$	0	0	0	0,4	0,4
r	2	5	5	5,52	5,52
m'	1	1	0,5	1,17	1,17
$D^{(2)}$	0,3 - 0,9			0,1 - 0,7	

Note 1: Onset of the compensating ramp expressed in duty ratio

Note 2: In increments of 0.1

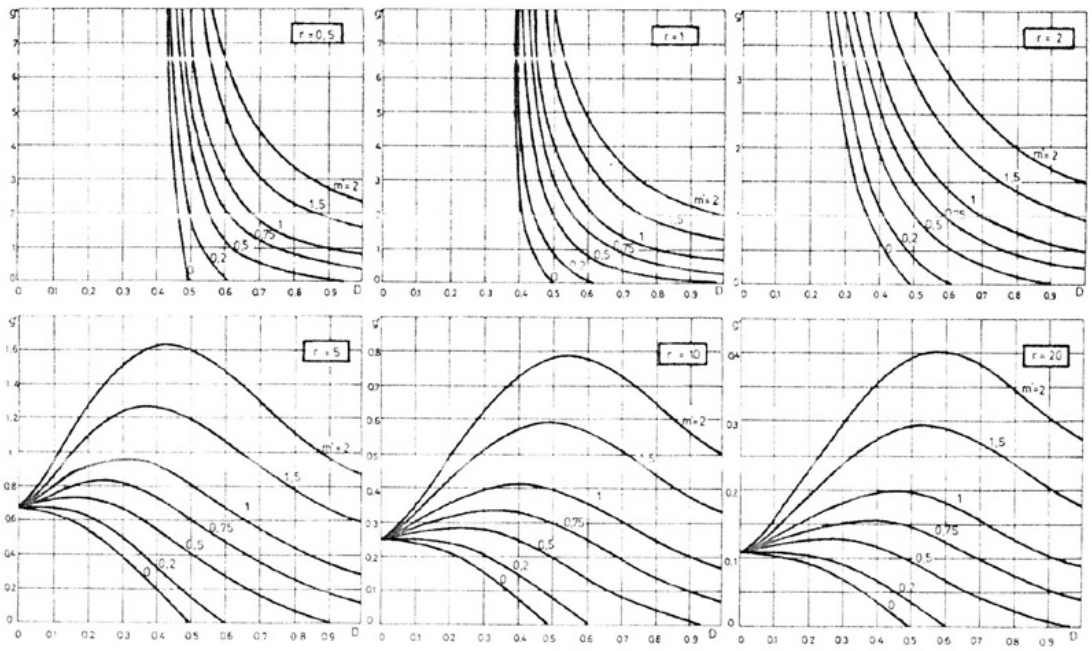

Fig.11. Normalized transconductances of the buck regulator at the verge of continuous subharmonic oscillation for different r and m' values

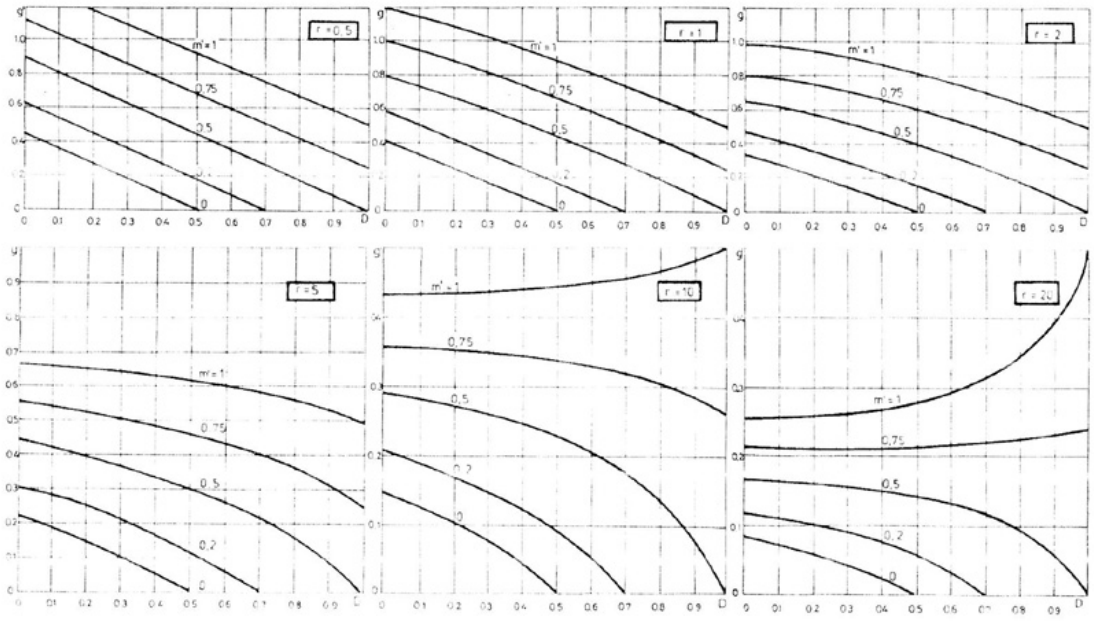

Fig.12. Normalized transconductances of the boost regulator at the verge of continuous subharmonic oscillation for different r and m' values.

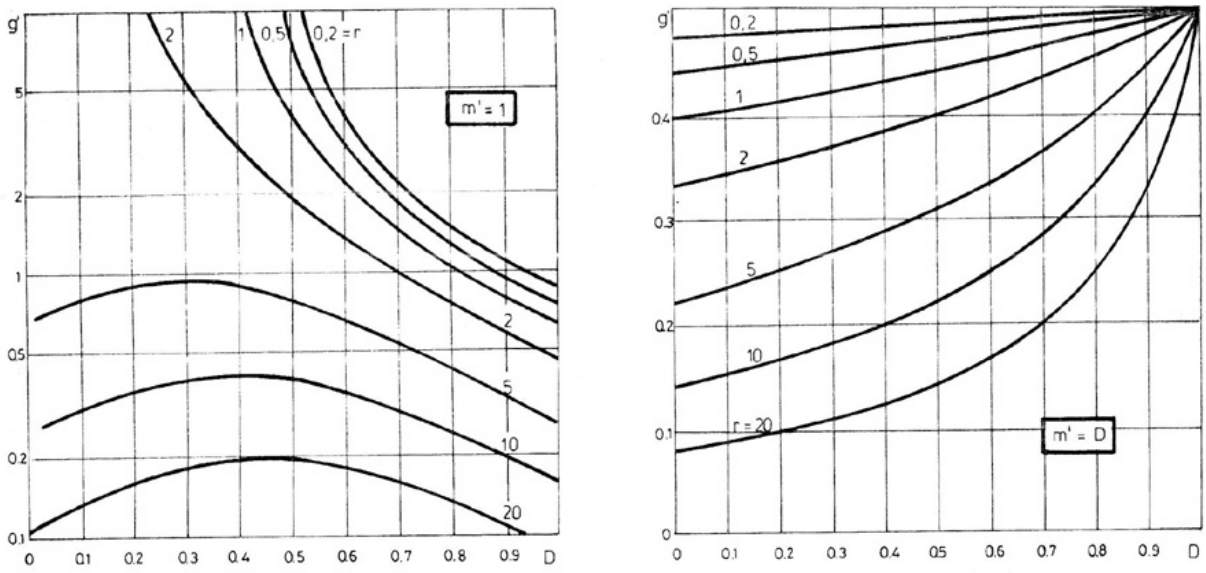

a./ buck b./ boost

Fig.13. Normalized transconductances of the buck and boost regulators at the verge of continuous subharmonic oscillation for different r values and with optimum compensating ramps.

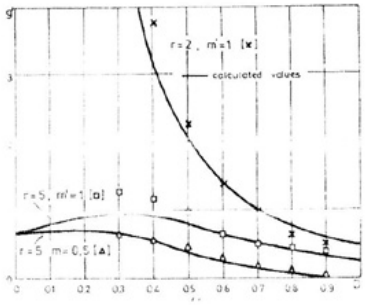

Fig.14. Measured and calculated boundaries of continuous subharmonic oscillation for buck converters.

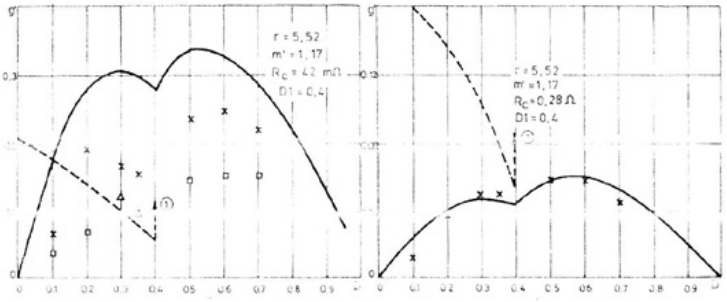

Fig.15. Measured and calculated boundaries of continuous and hysteretic subharmonic oscillation for a boost converter.

Fig.16. Measured and calculated upper boundaries of hysteretic subharmonic oscillation for a boost converter.

——— calculated upper limit, hysteretic oscillation
----- calculated limit, continuous oscillation
x measured upper limit, hysteretic oscillation
□ measured lower limit, hysteretic oscillation
Δ measured limit, continuous oscillation
Note 1: calculated limit of continuous oscillation above D = 0.4 (g' ≈ 0,68)

At the buck converter the onset of the compensating linear ramp was the beginning of the period and at the boost converter the linear ramp started at 40% of the period.

Measured boundaries of continuous instability for the buck converter are shown in Fig.14. together with the predictions of theory. It can be seen that the agreement between experimental and theoretical results is excellent for the case of m'=0,5 and very good for the case of m'=1.

Figs.15. and 16 display the results of measurements carried out on boost converters. Fig.15. shows the case when in part of the duty ratio range the boundary of continuous instability runs below the boundary of hysteretic instability. At D=0.4 the compensating ramp enters and this pushes the boundary of continuous instability well above the other boundary. Here the agreement between theory and experiment is only fair but this can be probably explained by the interaction of the two different instability mechanisms. At Fig.16. the upper boundary of the hysteretic instability is below the boundary of continuous instability. The agreement here is again excellent.

6. SUMMARY AND CONCLUSIONS

The analysis of high-frequency instabilities in the constant-frequency current-mode controlled converters has been extended to duty ratios above 50% in the paper. Above 50% stable operation is possible only by employing a compensating ramp. The optimum form of this ramp depends on the type of the converter: for the buck family it is of linear shape, for the boost family it is of parabolic shape. There is possibility for two different high-frequency instabilities at this controlling method. The first one, the continuously arising instability, can be present both in the buck and boost or buck-boost converters, while the hysteretic instability is characteristic only for the boost and buck-boost converters. The loop gain at the verge of continuous instability can be determined by perturbation analysis. The gain at the boundary of hysteretic instability can be calculated by investigating the switch-over conditions of the current comparator in the controller. Continuous instability depends on the slope of the compensating ramp and hysteretic instability depends on the actual value of the ramp.

Diagrams, presenting loop gain limits for stable operation, algorithm for the design of stable loops, and experimental results make the paper complete.

REFERENCES

[1] R.Redl, I. Novak, "Instabilities in Current-Mode Controlled Switching Voltage Regulators," PESC '81 Record (IEEE Publication 81CH1652-7), pp. 17-28.

[2] E.Pivit, J. Saxarra, "On Dual Control Pulse-Width Modulators for Stable Operation of Switched-Mode Power Supplies," Wiss. Ber. AEG-TELEFUNKEN, vol. 52 (1979), no.5, pp. 243-249.

[3] Shi-Ping Hsu et al, "Modelling and Analysis of Switching DC-to-DC Converters in Constant-Frequency Current-Programmed Mode," PESC '79 Record (IEEE Publication 79CH1461-3 AES), pp. 284-301.

[4] A. Capel, M. Clique, A.J. Fossard, "Current-Control Modulators - General Theory for Specific Designs," ESA Journal, 1980. vol.4. no.4. pp. 397-416.

[5] F.C. Lee, R.A. Carter, "Investigations of Stability and Dynamic Performances of Switching Regulators Employing Current-Injected Control," PESC '81 Record (IEEE Publication 81CH1652-7), pp. 3-16.

[6] B.E. Andersen et al, "Analysis of the Static Characteristics and Dynamic Response of Push-Pull Switching Converters Operating in the Current Programmed Mode," PESC '81 Record (IEEE Publication 81CH1652-7), pp. 29-38.

[7] R. Redl, I. Novak, "Stability Analysis of Constant-Frequency Current-Mode Controlled Power Converters," Proceedings of the Second International Powerconversion Conference, 1980, Munich, pp. 4.B.2-1 to 4.B.2-14.

[8] R. Redl, "Comparative Analysis of Overload Protection Methods for Switching-Mode Voltage Regulators," Proceedings of the Third ESTEC Spacecraft Power Conditioning Seminar (ESA Publication SP 126), 1977, pp. 155-164.

[9] C. Deisch, "Simple Switching Control Method Changes Power Converter into a Current Source," PESC '78 Record (IEEE Publication 78CH1337-AES), pp. 300-306.

[10] R. Redl, N.O. Sokal, "Optimizing Dynamic Behavior with Input and Output Feed-Forward and Current-Mode Control," Proceedings of POWERCON 7, 1980, San Diego, pp. H1-1 to H1-16.

TABLE 5. TRANSCONDUCTANCES AT THE START AND AT THE STOP OF HYSTERETIC SUBHARMONIC OSCILLATION

		starting value	ceasing value
Buck	constant off-time		
	infinite		$\left(\frac{T_{off}}{2C_o} + R_c\right)^{-1}$
	constant frequency		
	infinite		$\left(\frac{T}{2C_o} - R_c\right)^{-1}$
Boost	constant off-time		
	static turn-on	$\left[\frac{LI_o}{V_oC_oD'} + R_c\left(\frac{LI_o}{V_oDD'T_{off}} - \frac{1}{2}\right)\right]^{-1}$	$\left(\frac{R_cLT_o}{V_oDD'T_{off}} + \frac{LI_o}{V_oC_oD'} + \frac{T_{off}}{2C_o}\right)^{-1}$
	dynamic turn-on	$\left(\frac{LI_o}{V_oC_oD'}\right)^{-1}$	$\left(R_c + \frac{LI_o}{V_oC_oD'} + \frac{T_{off}}{2C_o}\right)^{-1}$
	constant frequency		
	static turn-on	$\left[\frac{LI_o}{V_oC_oD'} + R_c\left(\frac{LI_o}{V_oDD'^2T} - \frac{1}{2}\right)\right]^{-1}$	$\left[\frac{R_cLI_o}{V_oDD'(1-2D)T} + \frac{LI_o}{V_oC_oD'} + \frac{R_cD}{1-2D} + \frac{T}{2C_o}\right]^{-1}$
	dynamic turn-on	$\left(\frac{LI_o}{V_oC_oD'}\right)^{-1}$	$\left(\frac{R_c}{1-2D} + \frac{LI_o}{V_oC_oD'} + \frac{T}{2C_o}\right)^{-1}$
Buck-boost	constant off-time		
	static turn-on	$\left[\frac{DLI_o}{V_oC_oD'} + R_c\left(\frac{LI_o}{V_oD'T_{off}} - \frac{1}{2}\right)\right]^{-1}$	$\left(\frac{R_cLI_o}{V_oD'T_{off}} + \frac{DLI_o}{V_oC_oD'} + \frac{T_{off}}{2C_o}\right)^{-1}$
	dynamic turn-on	$\left(\frac{DLI_o}{V_oC_oD'}\right)^{-1}$	$\left(R_c + \frac{DLI_o}{V_oC_oD'} + \frac{T_{off}}{2C_o}\right)^{-1}$
	constant frequency		
	static turn-on	$\left[\frac{DLI_o}{V_oC_oD'} + R_c\left(\frac{LI_o}{V_oD'^2T} - \frac{1}{2}\right)\right]^{-1}$	$\left[\frac{R_cLI_o}{V_oD'(1-2D)T} + \frac{DLI_o}{V_oC_oD'} + \frac{R_cD}{1-2D} + \frac{T}{2C_o}\right]^{-1}$
	dynamic turn-on	$\left(\frac{DLI_o}{V_oC_oD'}\right)^{-1}$	$\left[\frac{R_c}{1-2D} + \frac{DLI_o}{V_oC_oD'} + \frac{(1-2D)T}{2C_o}\right]^{-1}$